ARTICLE

Microporous Silica Thin Films with Low Refractive Indices and High Young's Modulus

Wataru Shimizu* and Yasushi Murakami

Division of Chemistry and Materials, Faculty of Textile Science and Technology, Shinshu University, 3-15-1 Tokida, Ueda, Nagano 386-8567, Japan

ABSTRACT A microporous silica thin film with low refractive index (low-*n*) of 1.27 and high Young's modulus of 19.5 GPa was obtained by sol−gel synthesis using hydroxyacetone catalyst with tetramethyl orthosilicate and water in ethanol. Transmission electron microscope images and nitrogen adsorption−desorption measurements showed that the pores in the synthesized silica were <1 nm in diameter. Unlike many other microporous synthesis methods, our method did not require sacrificial reagents as templates. This allowed low-temperature fabrication of high-strength low-*n* silica.

KEYWORDS: refractive index • low-*k* • dielectric constant • antireflection • porosity • template free • catalytic sol−gel process

INTRODUCTION

Low refractive index (low-*n*) thin films have been employed as antireflective (AR) coatings for optical applications including display devices, lenses, and solar cells (1−10). Magnesium fluoride is a low-*n* ($n = 1.38$) material that is widely used in commercial applications. Films with lower indices (e.g., $n < 1.3$) are desired for obtaining high transmittance. Such films may be attained by incorporation of nanosized pores filled with air having $n = 1.0$. However, preparation of magnesium fluoride with nanosized pores is not trivial.

A promising candidate is highly porous silica, which can be in the form of particles (2, 4, 8), xerogel (12, 13), or aerogel (11, 14). Silica has a low-*n* ($n = 1.46$), good durability, and environmental resistance (7, 19) and can be used for optical applications, microelectronics (15−18), and thermal applications (14). However, increasing the content of nanosized pores is generally expected to greatly deteriorate the mechanical strength of the film (11). This problem has stimulated many studies (16, 17, 20−22) regarding reinforcement of porous silica materials. For example, Reidy et al. reported that fluorination of silica improved the mechanical strength of porous silica. The resultant film had an average pore size of about 20 nm, elastic modulus of 14 GPa, and $n = 1.24$ (20). Luo et al. reinforced porous silica with colloidal silica nano particles (22), yielding a film with a low-*n* of 1.28, Young's modulus of 16.6 GPa, and hardness of 0.92 GPa. Although high-density spherical silica nanoparticles should have high hardness, their introduction into the film matrix may roughen the surface and cause terrible increment of light scattering. Further improvement of these films in terms of their Young's modulus and transparency is quite necessary. Investigations focusing on pore structures, pore uniformity and film formation process will be helpful for obtaining stronger and more transparent films.

Porous silica is typically mesoporous (8, 11, 16, 17) with pores 2−50 nm in diameter (23). As shown in recent investigations, formation of micropores <2 nm in diameter (23) would be favorable in order to increase the mechanical strength (24−26). Furthermore, micropores would probably eliminate penetration and adsorption of chemical species (21), which give rise to light scattering and absorption. As for microporous silica film is well-known as packed silica nanoparticles (27−31) and monolithic microporous silica (32−41). Silica is promising high optical transparency, but nanoparticles tend to form inhomogeneous aggregation during packing process, which causes nonuniform density distribution and light scattering. In addition, pore volume fraction of dead space in packed silica nanoparticles is limited because of its formation principle. On the other hand, monolithic microporous silica consists of solid skeleton and void structure, which is usually prepared by template technique using organic-functionalized silicon alkoxides (32, 33, 35, 41) or additive organic precursors (37−40, 42) to create the pores. However, heat treatment above 400 °C to remove these organics and form micropores inevitably results in collapse of pores itself. This contracts the film, which increases the film density and *n*. Moreover, residual organic functional groups or additives also increase *n*. Alternative processes of the monolithic microporous silica fabrication are still worth investigation.

In an earlier study, we developed a catalytic sol−gel process using tetramethyl orthosilicate (TMOS) and the nonionic catalyst hydroxyacetone (43). In this study, we applied this method to fabricate microporous silica thin film with low-*n* and high Young's modulus. The homogeneous reaction with the nonionic catalyst facilitates production of highly porous monolithic microporous silica with uniform pores <1 nm in diameter. Because this process requires no sacrificial templates, residual alkoxy groups and the catalyst are easily removed during hydrolysis. Additionally, the

* Corresponding author. E-mail: wats@shinshu-u.ac.jp.
Received for review July 14, 2010 and accepted October 11, 2010

DOI: 10.1021/am100612g

Published on Web 10/27/2010

Table 1. Summary of the Preparation Process for Each of the Silica Films and Powders

sample code	chemical hydrolysis[a]	heat treatment temperature (°C)
HMS_{80}	yes	80
HMS_{150}	yes	150
HMS_{200}	yes	200
HMS_{250}	yes	250
HMS_{300}	yes	300
MS_{200}	no	200

[a] The film and powder samples were chemically hydrolyzed by immersing them in water at 80 °C before heat treatment.

process temperature can be as low as 80 °C, which results in less thermal stress. This also prevents the pore structures from collapsing, which aids in production of uniform pores with large volumes.

EXPERIMENTAL SECTION

Synthesis. To produce the film coating solution, TMOS ($Si(OCH_3)_4$, Tokyo Chemical Industry, > 98%), ethanol (Wako, > 99.5%), distilled water, and hydroxyacetone (CH_3COCH_2OH, Tokyo Chemical Industry, > 80%) were mixed thoroughly at 25 °C for 2 days, and then kept at 40 °C for 3 days. The molar ratio of $Si(OCH_3)_4$:H_2O:C_2H_5OH:CH_3COCH_2OH was 1:5:27.5:1. Si(100) substrates were coated with the silica sol by spin coating at 2000 rpm for 60 s at 25 °C, and dried at 25 °C for a day. The dried silica films were then either heated at 200 °C for 2 h (nonhydrolyzed film, MS_{200}), or immersed in water at 80 °C for 2 h to chemically hydrolyze the methoxy groups and remove organic compounds. After chemical hydrolysis, the films were dried and heated at 80−300 °C for 2 h (HMS_{80-300}) to promote the condensation reaction of silanol groups and eliminate pore water. Table 1 summarizes the preparation conditions for each sample.

Characterization. The *n* and film thickness were measured with a spectroscopic ellipsometer (Horiba Jobin Yvon, UVISEL M200) at 80 °C, which minimized water adsorption. The mass fraction of water in the film prepared with hydrolysis but no heating was estimated to be approximately 15% by thermogravimetric analysis. A flake of the film was observed using a transmission electron microscope (TEM, JEOL, JEM-2010) with an acceleration voltage of 200 kV. The surface morphology and the cross-section of a typical film were observed using a field-emission scanning electron microscope (FE-SEM, Hitachi, S-5000) and an atomic force microscope (AFM, Seiko Instruments, SPA400). The pore volume and surface area of the dried silica coating solution was evaluated by nitrogen gas adsorption−desorption measurement (Micromeritics, ASAP2010). Micropore volume and surface area were calculated from adsorption isotherm data using the *t*-plot method (0.35 nm < *t* < 0.5 nm) (39, 46). Total pore volumes were determined from the volume of adsorbed nitrogen gas at a relative pressure of 0.95 (23). The pore size distributions were determined by the Saito−Foley (SF) modified Horváth−Kawazoe (HK) model from adsorption isotherms in the low relative pressure region. The HK model (44) describes a semiempirical calculation of the pore size distribution from the nitrogen adsorption isotherm in microporous materials with slitlike pores, and is applicable to active carbon. The SF-modified HK model (45) extends application to the cylindrical pore geometry of microporous materials such as zeolite and silica, which have been used in many studies of microporous silica (41, 46, 47). A Fourier transform infrared spectrophotometer (FT-IR, Perkin-Elmer 1650) was used to record spectra of the dried silica sol mixed with KBr from 4000 to 450 cm^{-1}.

The mechanical properties of the films were measured at room temperature by nanoindentation (Agilent Technologies NanoIndenter G200, Berkovich diamond indenter) based on ISO-14577 (48). Sixteen points on each sample were assayed using the continuous stiffness measurement (CSM), and the average and standard deviation were calculated. The first 10% of the film thickness was used as the indentation depth range to determine Young's modulus and hardness, and the values were compared with corresponding results from other samples. The Poisson ratio of silica films is 0.25 as calculated using Young's modulus.

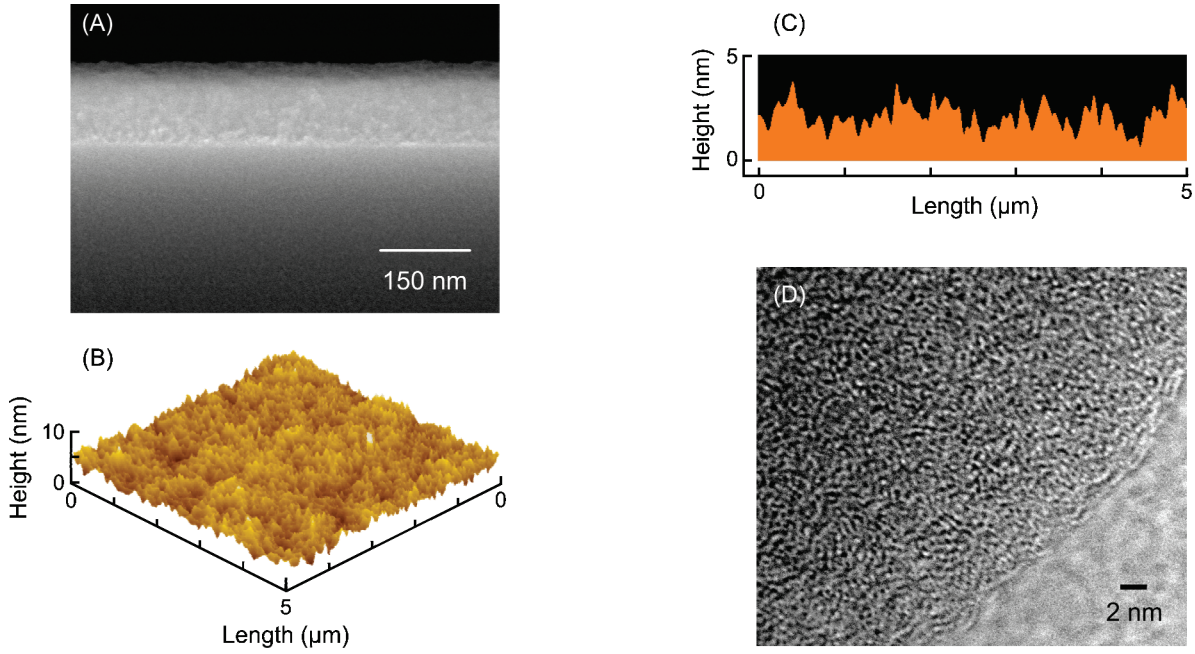

FIGURE 1. Typical images of the silica film HMS_{250}: (A) cross-sectional SEM image, (B) AFM image, (C) cross-sectional AFM profile measured along the indicated plane, and (D) TEM image.

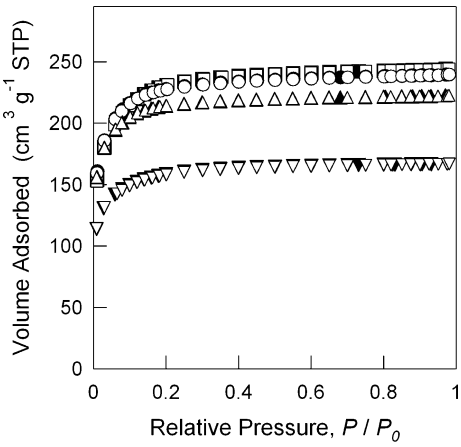

FIGURE 2. Nitrogen adsorption−desorption isotherms of the chemically hydrolyzed silica powders heat-treated at different temperatures (HMS_{150} (circle), HMS_{200} (square) and HMS_{300} (triangle)) and the nonhydrolyzed silica heat-treated at 200 °C (MS_{200} (inverted triangle)). Adsorption isotherms are represented by open symbols and desorption isotherms by solid symbols.

RESULTS AND DISCUSSION

Figure 1A shows a typical FE-SEM cross-sectional image of the silica film HMS_{250}. The film thickness was estimated at approximately 125 nm. In the AFM image (Figure 1B) and cross-sectional AFM profile (Figure 1C) the film appeared very smooth with small ridges approximately 3 nm in height. The morphology of the micropores was undetectable by FE-SEM and AFM, due to the size (<2 nm diameter) of the pores. Pores of approximately 0.5 nm in diameter with a narrow size distribution were observed in the TEM image of a typical flake of silica film (Figure 1D).

Nitrogen gas adsorption−desorption isotherms of the silica powders HMS_{150}, HMS_{200}, HMS_{300} and MS_{200} (Figure 2) were used to classify them as IUPAC type I with monolayer adsorption of N_2 (23), which probably contains micropores with diameters <2 nm. The isotherm of the silica powder HMS_{250} had significant overlap with that of HMS_{300}, and consequently HMS_{250} is not depicted in Figure 2. In the *t*-plot (Figure 3A) calculated from nitrogen adsorption isotherm data for HMS_{200} the curve did not pass through the origin and had a positive *y*-intercept, which indicates HMS_{200} is microporous. The specific surface area of a micropore in HMS_{200} was calculated to be 470 $m^2\ g^{-1}$, and the pore volume was calculated to be 0.21 $cm^3\ g^{-1}$. The pore size distribution in HMS_{200} (Figure 3B) is the narrowest of all reported microporous silica (32, 34−36, 39).

The total pore volume for the hydrolyzed silica powder HMS_{150} was 0.37 $cm^3\ g^{-1}$ (Table 2). Little change in the pore volume was observed when the hydrolyzed silica powders were heated at 200 °C (0.38 $cm^3\ g^{-1}$), 250 °C (0.34 $cm^3\ g^{-1}$), and 300 °C (0.34 $cm^3\ g^{-1}$). The pore volume for the nonhydrolyzed silica powder MS_{200} (0.26 $cm^3\ g^{-1}$) was smaller than that for the hydrolyzed silica HMS_{200} (0.38 $cm^3\ g^{-1}$). The pore volume fraction is related to the refractive index according to the Lorentz−Lorenz equation (6, 8, 12), and this explains that the increasing of the pore volume decreases the refractive index. In order to enhance the specific pore volume value, we developed the synthesis procedure in which ethanol was used as the solvent instead of methanol (43), achieving the increase of maximum pore volume from 0.33 to 0.38 $cm^3\ g^{-1}$ without expanding pore diameter.

We believe that the homogeneous hydrolysis reaction in the presence of hydroxyacetone catalyst facilitates formation of micropores. The framework of micropores might have already been fabricated in silica precursors in the coating solution. The dried silica coating solution includes a lot of micropores, and therefore, all of the silica powders consid-

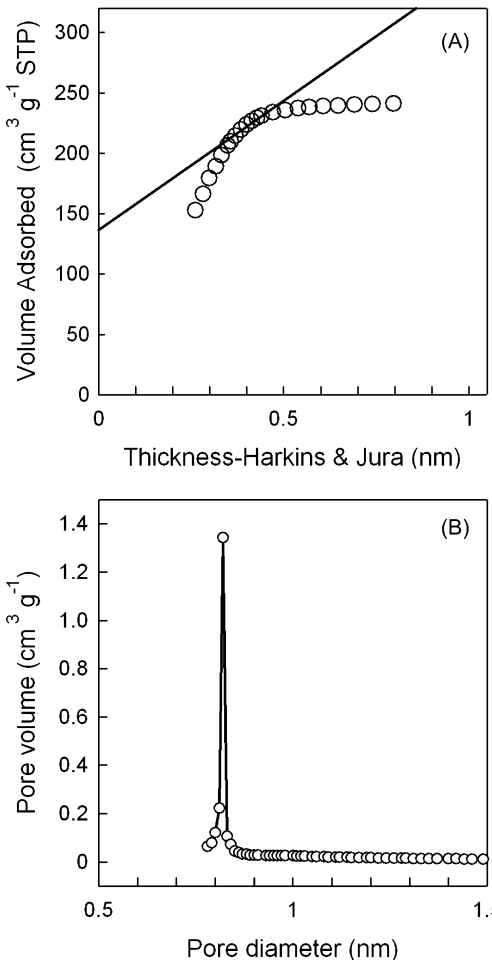

FIGURE 3. (A) *t*-Plot curve and (B) pore size distribution of the hydrolyzed silica powder HMS_{200}.

Table 2. Structural Properties and Refractive Indices of the Microporous Silica Samples[a]

sample code	S_{micro}[b] ($m^2\ g^{-1}$)	V_{micro}[b] ($m^3\ g^{-1}$)	V_{total}[b] ($m^3\ g^{-1}$)	n_{633}[c]	t[c] (nm)
HMS_{80}	N/A	N/A	N/A	1.340	132
HMS_{150}	575	0.26	0.37	1.319	135
HMS_{200}	470	0.21	0.38	1.278	130
HMS_{250}	482	0.22	0.34	1.270	128
HMS_{300}	532	0.24	0.34	1.265	130
MS_{200}	350	0.16	0.26	1.358	162

[a] Notation: S_{micro}, micropore surface area; V_{micro}, micropore volume; V_{total}, total pore volume; n_{633}, refractive index at 633 nm; t, film thickness. [b] Powder samples were evaluated. [c] Film samples were estimated by ellipsometric measurement.

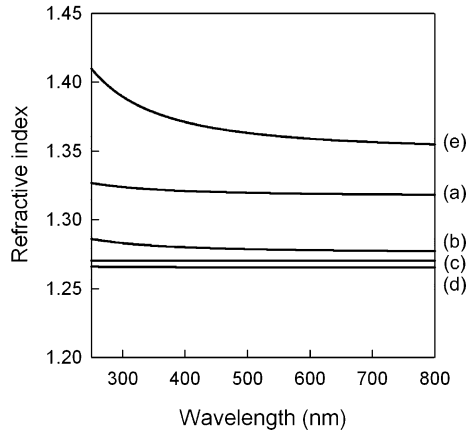

FIGURE 4. Refractive index as a function of wavelength for (a) HMS_{150}, (b) HMS_{200}, (c) HMS_{250}, (d) HMS_{300}, and (e) MS_{200}.

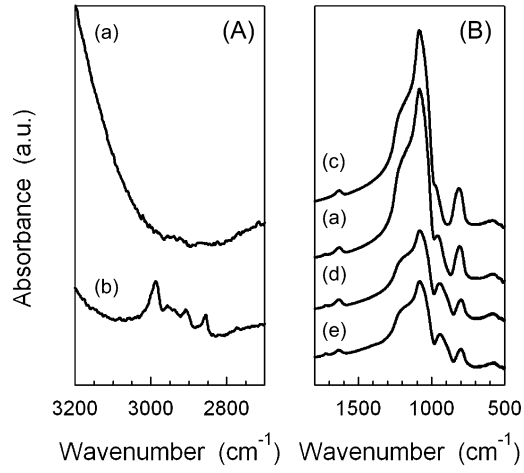

FIGURE 5. (a)FT-IR spectra of the hydrolyzed silica film HMS_{200}, (b) the nonhydrolyzed silica film MS_{200}, and the hydrolyzed silica films (c) HMS_{250}, (d) HMS_{150}, and (e) HMS_{80}.

ered in this work had large pore volume. High-temperature heating should cause densification with the condensation reaction, and consequently the total pore volumes of the silica powders heated at ≥250 °C were smaller than those of HMS_{150} and HMS_{200}.

Film thickness and n for each silica film are summarized in Table 2. Within the wavelength range 250−800 nm, the n were lower for the hydrolyzed films than the nonhydrolyzed film (Figure 4). Figure 5A compares the FT-IR absorption spectra from 3200−2700 cm^{-1} for HMS_{200} and MS_{200}. Peaks at 2980 and 2860 cm^{-1} for the C−H stretching mode of CH_3 and CH_2, respectively (17), were observed in the spectra of MS_{200} but not HMS_{200}. This suggests that organics, such as methoxy groups and hydroxyacetone, remained in the nonhydrolyzed silica but were removed during the process of chemical hydrolysis. The absence of these organics definitely facilitates reduction of n and increases the pore volume of the hydrolyzed films.

The n of the hydrolyzed film decreased as the temperature for heat treatment was increased to 250 °C. The dependence of the n on wavelength changed with the temperature the film was heated at. When the hydrolyzed silica film was heated at 250 or 300 °C, the n was independent of the wavelength. The FT-IR absorption spectra from 1800−500 cm^{-1} of the hydrolyzed silica films HMS_{80}, HMS_{150}, HMS_{200} and HMS_{250} are compared in Figure 5B. The absorption band near 950 cm^{-1} can be attributed to stretching vibrations of the Si−OH bonds (8, 12), and is observed in the spectra of HMS_{80}, HMS_{150}, and HMS_{200}. The peak height for the asymmetric stretching vibration of Si−O−Si (TO_3 mode) at about 1080 cm^{-1} (8, 12, 17) increased with increasing heating temperature. In contrast, the Si−OH peak height decreased with increasing heating temperature, and was not apparent in the spectrum of HMS_{250}. These results suggest that the terminal silanol groups were almost completely converted to Si−O−Si bonds with thermal dehydroxylation and condensation (49) at 250 °C.

Although the total pore volume decreased when the heating temperature was ≥250 °C, the n of HMS_{250} was lower than that of HMS_{200} (Table 2). This is due to a reduction in the absorption of water for the high-temperature film. Typically, hydrophilic silanol groups aid adsorption of water, and high polarization of water and silanol groups must increase the n of the film (7, 16, 24). When the film is heated at ≥250 °C, the number of terminal Si−OH is decreased (Figure 5B), which should reduce the adsorption of water and decrease n to <1.3.

As discussed earlier, the pore volume of the hydrolyzed silica powder HMS_{250} was 0.34 cm^3 g^{-1}. A pore volume fraction of 42.8% was calculated using the density of dense silica (2.20 g cm^{-3}). This was used to calculate $n = 1.23$ by substituting $n = 1.46$ for dense silica into the Lorentz−Lorenz equation (6, 8, 12). The experimental n of 1.27, which was determined by ellipsometric measurement (Table 2), is larger than the calculated n, which should be due to residues such as water in the experimental film.

Mechanical strengths were determined for the hydrolyzed silica film HMS_{300}. In consideration of the substrate effect, two different thicknesses of 125 and 240 nm were adopted. Young's modulus was 19.4 ± 0.91 GPa and the hardness was 0.45 ± 0.03 GPa at an indentation depth of 12.5 nm for the 125 nm thick film, whereas the corresponding values were 19.5 ± 0.91 GPa and 0.74 ± 0.04 GPa at an indentation depth of 24 nm for the 240 nm thick film (Figure 6).

Young's modulus of this film is the highest of all reported porous silica thin films with equivalent porosity or n (16, 17, 20−22, 26, 31, 50). In this work, tetrafunctional silicon alkoxide was used as a reagent for the microporous silica film. This reagent produced more cross-linking bonds between pore structures than trifunctional alkoxides and reagents containing alkyl groups, such as triethoxyfluorosilane (16, 20) and silsesquioxane (21, 26, 42). Moreover, unreacted methoxy groups and silanol groups were not present in the hydrolyzed silica powder heated at >250 °C, and instead these formed Si−O−Si bonds (Figure 5A,B). These results indicate the chemical hydrolysis and thermal condensation increased the bonding between the micropores and made the film stronger. At the same porosity,

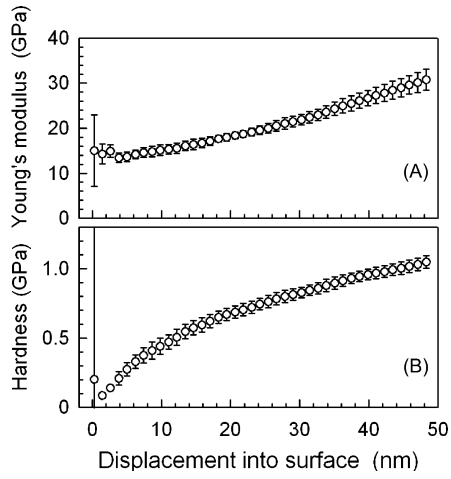

FIGURE 6. (A) Young's modulus and (B) hardness values of HMS_{300} as a function of the indentation depth from surface. The thickness of the silica film used in this study was 240 nm.

the density in number of walls per unit volume in a microporous material is higher than in a mesoporous material. Consequently, because stress acting on a material might disperse into the walls, it is expected that this stress is reduced in a microporous material compared with a mesoporous material. As a result, the pore structure in a microporous material should not collapse as easily as in a mesoporous material. A recent theoretical study has revealed that uniformity of pore diameter increases elastic modulus of silica thin film (51). Therefore, the uniform pores of the hydrolyzed silica film result in a homogeneous wall density distribution, which provides high resistance to elastic variation.

CONCLUSIONS

Low-n ($n < 1.3$) was achieved with the introduction of large volume micropores in silica films. Film preparation utilized the sol−gel process with the catalyst hydroxyacetone. A low-n ($n = 1.27$) was facilitated by removal of organic functional groups and the catalyst during the process of hydrolysis, and of adsorbed water and OH groups by heating (250−300 °C). The films have very small pores, which could protect against absorption or penetration of pollutants and other materials. Furthermore, due to their high Young's modulus (>15 GPa) these films are robust.

Acknowledgment. This work was supported by CLUSTER (the second stage) of the Ministry of Education, Culture, Sports, Science and Technology, Japan. We thank TOYO Corporation for the nanoindentation measurements of the microporous silica films.

REFERENCES AND NOTES

(1) Yoldas, B. E. *Appl. Opt.* **1980**, *19*, 1425–1433.
(2) Thomas, I. M. *Appl. Opt.* **1992**, *31*, 6145–6149.
(3) Ibn-Elhaj, M.; Schadt, M. *Nature* **2001**, *410*, 796–799.
(4) Prevo, B. G.; Hwang, Y.; Velev, O. D. *Chem. Mater.* **2005**, *17*, 3642–3651.
(5) Xi, J.-Q.; Kim, J. K.; Schubert, E. F. *Nano Lett.* **2005**, *5*, 1385–1387.
(6) Cho, J.; Hong, J.; Char, K.; Caruso, F. *J. Am. Chem. Soc.* **2006**, *128*, 9935–9942.
(7) Konjhodzic, D.; Schroter, S.; Mariow, F. *Phys. Status Solidi A* **2007**, *204*, 3676–3688.
(8) Vincent, A.; Babu, S.; Brinley, E.; Karakoti, A.; Deshpande, S.; Seal, S. *J. Phys. Chem. C* **2007**, *111*, 8291–8298.
(9) Chhajed, S.; Schubert, M. F.; Kim, J. K.; Schubert, E. F. *Appl. Phys. Lett.* **2008**, *93*, 251108.
(10) Hoshikawa, Y.; Yabe, H.; Nomura, A.; Yamaki, T.; Shimojima, A.; Okubo, T. *Chem. Mater.* **2010**, *22*, 12–14.
(11) Leventis, N.; Sotiriou-Leventis, C.; Zhang, G. H.; Rawashdeh, A.-M. M. *Nano Lett.* **2002**, *2*, 957–960.
(12) Falcaro, P.; Grosso, D.; Amenitsch, H.; Innocenzi, P. *J. Phys. Chem. B* **2004**, *108*, 10942–10948.
(13) Zhou, Y.; Schattka, J. H.; Antonietti, M. *Nano Lett.* **2004**, *4*, 477–481.
(14) Hrubesh, L. W.; Pekala, R. W. *J. Mater. Res.* **1994**, *9*, 731–738.
(15) Jain, A.; Rogojevic, S.; Ponoth, S.; Agarwal, N.; Matthew, I.; Gill, W. M.; Persans, P.; Tomozawa, M.; Plawsky, J. L.; Simonyi, E. *Thin Solid Films* **2001**, *398*, 513–522.
(16) Gorman, B. P.; Orozco-Teran, R. A.; Roepsch, J. A.; Dong, H.; Reidy, R. F. *Appl. Phys. Lett.* **2001**, *79*, 4010–4012.
(17) Chen, J. Y.; Pan, F. M.; Cho, A. T.; Chao, K. J.; Tsai, T. G.; Wu, B. W.; Yang, C. M.; Chang, L. *J. Electrochem. Soc.* **2003**, *150*, F123–F127.
(18) Ro, H. W.; Peng, H.; Niihara, K.; Lee, H. J.; Lin, E. K.; Karim, A.; Gidley, D. W.; Jinnai, H.; Yoon, D. Y.; Soles, C. L. *Adv. Mater.* **2008**, *20*, 1934–1939.
(19) Biswas, P. K.; Devi, P. S.; Chakraborty, P. K.; Chatterjee, A.; Ganguli, D.; Kamath, M. P.; Joshi, A. S. *J. Mater. Sci. Lett.* **2003**, *22*, 181–183.
(20) Dong, H.; Gorman, B. P.; Zhang, Z.; Orozco-Teran, R. A.; Roepsch, J. A.; Mueller, D. W.; Kim, M. J.; Reidy, R. F. *J. Non-Cryst. Solids* **2004**, *350*, 345–350.
(21) Cha, B. J.; Kim, S.; Char, K.; Lee, J.-K.; Yoon, D. Y.; Rhee, H.-W. *Chem. Mater.* **2006**, *18*, 378–385.
(22) Luo, J.-T.; Wen, H.-C.; Chang, Y.-M.; Wu, W.-F.; Chou, C.-P. *J. Colloid Interface Sci.* **2007**, *305*, 275–279.
(23) Sing, K. S. W.; Everett, D. H.; Haul, R. A. W.; Moscou, L.; Pierotti, R. A.; Rouquérol, J.; Siemieniewska, T. *Pure Appl. Chem.* **1985**, *57*, 603–619.
(24) Hatton, B. D.; Landskron, K.; Hunks, W. J.; Bennett, M. R.; Shukaris, D.; Perovic, D. D.; Ozin, G. A. *Mater. Today* **2006**, *9*, 22–31.
(25) Xia, Z.; Riester, L.; Sheldon, B. W.; Curtin, W. A.; Liang, J.; Yin, A.; Xu, J. M. *Rev. Adv. Mater. Sci.* **2004**, *6*, 131–139.
(26) Gaire, C.; Ou, Y.; Arao, H.; Egami, M.; Nakashima, A.; Picu, R. C.; Wang, G.-C.; Lu, T. -M. *J. Porous Mater.* **2010**, *17*, 11–18.
(27) Chu, L.; Tejedor-Tejedor, M. I.; Anderson, M. A. *Microporous Mater.* **1997**, *8*, 207–213.
(28) Meixner, D. L.; Gilicinski, A. G.; Dyer, P. N. *Langmuir* **1998**, *14*, 3202–3209.
(29) Colomer, M. T.; Anderson, M. A. *J. Non-Cryst. Solids* **2001**, *290*, 93–104.
(30) Kremer, S. P. B.; Kirschhock, C. E. A.; Tielen, M.; Collignon, F.; Grobet, P. J.; Jacobs, P. A.; Martens, J. A. *Adv. Funct. Mater.* **2002**, *12*, 286–292.
(31) Groen, J. C.; Peffer, L. A. A.; Pérez-Ramírez, J. *Microporous Mesoporous Mater.* **2003**, *60*, 1–17.
(32) Brinker, C. J.; Ward, T. L.; Sehgal, R.; Raman, N. K.; Hietala, S. L.; Smith, D. M.; Hua, D. W.; Headley, T. J. *J. Membr. Sci.* **1993**, *77*, 165–179.
(33) Raman, N. K.; Brinker, C. J. *J. Membr. Sci.* **1995**, *105*, 273–279.
(34) Nair, B. N.; Elferink, J. W.; Keizer, K.; Verweij, H. *J. Sol−Gel Sci. Technol.* **1997**, *8*, 471–475.
(35) Lu, Y.; Cao, G.; Kale, R. P.; Prabakar, S.; López, G. P.; Brinker, C. J. *Chem. Mater.* **1999**, *11*, 1223–1229.
(36) Lu, Y.; Fan, H.; Doke, N.; Loy, D. A.; Assink, R. A.; LaVan, D. A.; Brinker, C. J. *J. Am. Chem. Soc.* **2000**, *122*, 5258–5261.
(37) Kruk, M.; Asefa, T.; Jaroniec, M.; Ozin, G. A. *J. Am. Chem. Soc.* **2002**, *124*, 6383–6392.
(38) Endo, A.; Miyata, T.; Akiya, T.; Nakaiwa, M.; Inagi, Y.; Nagamine, S. *J. Mater. Sci.* **2004**, *39*, 1117–1119.
(39) Di, Y.; Meng, X.; Wang, L.; Li, S.; Xiao, F.-S. *Langmuir* **2006**, *22*, 3068–3072.
(40) Wang, R.; Han, S.; Hou, W.; Sun, L.; Zhao, J.; Wang, Y. *J. Phys. Chem. C* **2007**, *111*, 10955–10958.
(41) Wei, Q.; Wang, F.; Nie, Z.-R.; Song, C.-L.; Wang, Y.-L.; Li, Q.-Y. *J. Phys. Chem. B* **2008**, *112*, 9354–9359.

(42) Lee, K. H.; Yim, J.-H.; Baklanov, M. R. *Microporous Mesoporous Mater.* **2006**, *94*, 113–121.
(43) Shimizu, W.; Matsumoto, T.; Hosoo, S.; Nagahira, H.; Murakami, Y. *J. Ceram. Soc. Jpn.* **2007**, *115*, 712–716.
(44) Horváth, G.; Kawazoe, K. *J. Chem. Eng. Jpn.* **1983**, *16*, 470–475.
(45) Saito, A.; Foley, H. C. *AIChE J.* **1991**, *37*, 429–436.
(46) Boury, B.; Corriu, R. J. P.; Strat, V. L. *Chem. Mater.* **1999**, *11*, 2796–2803.
(47) Hawkins, K. M.; Wang, S. S.-S.; Ford, D. M.; Shantz, D. F. *J. Am. Chem. Soc.* **2004**, *126*, 9113–9119.
(48) *ISO 14577—1:2002, Metallic materials—Instrumented indentation test for hardness and materials parameters—Part 1: Test method*; International Organization for Standardization: Geneva, Switzerland, 2002.
(49) Brinker, C. J.; Scherer, G. W. In *Sol—Gel Science, The Physics and Chemistry of Sol—Gel Processing*; Academic Press: New York, 1990.
(50) Takada, S.; Hata, N.; Seino, Y.; Fujii, N.; Kikkawa, T. *J. Appl. Phys.* **2006**, *100*, 123512.
(51) Miyoshi, H.; Hata, N.; Kikkawa, T. *Jpn. J. Appl. Phys.* **2005**, *44*, 1166–1168.

AM100612G